Geophysical Journal International

*Geophys. J. Int.* (2017) **208,** 1237–1249
Advance Access publication 2016 December 5
GJI Seismology

doi: 10.1093/gji/ggw454

# Post-seismic velocity changes along the 2008 *M*7.9 Wenchuan earthquake rupture zone revealed by *S* coda of repeating events

Le Li,[1] Fenglin Niu,[2,3] Qi-Fu Chen,[4] Jinrong Su[5] and Jiabin He[6]

[1]*Key Laboratory of Earthquake Prediction, Institute of Earthquake Science, China Earthquake Administration, Beijing, China*
[2]*State Key Laboratory of Petroleum Resource and Prospecting, and Unconventional Natural Gas Institute, China University of Petroleum, Beijing, China*
[3]*Department of Earth Science, Rice University, Houston, TX, USA. E-mail: niu@cup.edu.cn*
[4]*Key Laboratory of Earth and Planetary Physics, Institute of Geology and Geophysics, Chinese Academy of Sciences, Beijing, China*
[5]*Earthquake Administration of Sichuan Province, Chengdu, China*
[6]*Earthquake Administration of Yunnan Province, Kunming, China*

Accepted 2016 December 2. Received 2016 November 26; in original form 2016 June 14

## SUMMARY

We investigated post-seismic velocity changes within the fault zone of the 2008 *M*7.9 Wenchuan earthquake using coda wave data of repeating small earthquakes. We employed template matching and grid search methods to identify well-defined repeating earthquakes in order to minimize artefacts induced by variations in source location. We identified a total of 12 isolated patches in the fault zone that ruptured more than twice in a 1 yr period after the *M*7.9 earthquake. We applied the coda wave interferometry technique to the waveform data of the 34 identified repeating earthquakes to estimate velocity changes between the first and subsequent events in each cluster. We found that major post-seismic velocity changes occurred in the southwestern part of the rupture area, where the main rupture was initiated and characterized by thrust motion, while the Beichuan area in the northeastern part of the rupture zone appears to experience very little post-seismic velocity changes.

**Key words:** Interferometry; Earthquake source observations; Earthquake interaction, forecasting, and prediction; Seismicity and tectonics; Coda waves; Wave scattering and diffraction.

## 1 INTRODUCTION

The 2008 May 12, $M_w$ 7.9 Wenchuan Earthquake, occurred along the Longmen Shan fault zone at the eastern margin of the Tibetan Plateau, was one of the most devastating intraplate earthquakes in this century. The low seismic activity and deformation rate estimated from GPS and geological data have led to an assessment of moderate seismic hazard for this region before the Wenchuan earthquake (e.g. Xu *et al*. 2009). Li *et al.* (2011) analysed repeating earthquake data before the Wenchuan earthquake and found that the deformation rates at seismogenic depths are much larger than the surface measurements, which may explain the odds about the occurrence of this unanticipated earthquake. Field geological investigations identified a 240 km long surface rupture zone along the Beichuan fault characterized by right-lateral oblique faulting (Beichuan rupture zone, thick red line in Fig. 1), and a 72 km long surface rupture zone along the Pengguan fault featured by dip-slip reverse faulting (Xiaoyudong rupture zone, thick blue line; Xu *et al*. 2009). The two rupture zones actually overlap, which are also illustrated by numerous aftershocks events (Fig. 1).

The physical processes associated with occurrence of earthquakes, such as coseismic stress changes, fluid migration, and the formation of damage zone at shallow depths, are likely to cause changes of rock properties within and around the rupture zones (e.g. Chen *et al*. 2010; Obermann *et al*. 2014). Both coseismic velocity drop and post-seismic velocity recovery were observed from continuous seismic noise data recorded by the Sichuan Regional Seismic Network (Cheng *et al*. 2010), the Western Sichuan Seismic Array (Chen *et al*. 2010; Froment *et al*. 2013; Obermann *et al*. 2014), and the Zipingpu Reservoir Seismic Network (ZRSN; Liu *et al*. 2014). By comparing velocity changes observed in different frequency bands, these authors were able to confirm changes related to permanent damage in the shallow crust (Liu *et al*. 2014), post-seismic deformation in the middle crust (Froment *et al*. 2013), as well as structural changes near the rupture areas of the Wenchuan main shock (Obermann *et al*. 2014). While continuous records of ambient noise data provide a great way for monitoring velocity changes, the technique, however, requires a great number of temporal stacking to obtain robust Greens' functions, which is challenging for high temporal resolution monitoring of subsurface velocity changes.

Repeating earthquakes are ruptures over the same fault patch with the same focal mechanism but different occurring time (e.g. Nadeau *et al*. 1995). Repeating events produce nearly identical seismograms when recorded at the same station, so that temporal changes in the medium can be more easily isolated from changes in

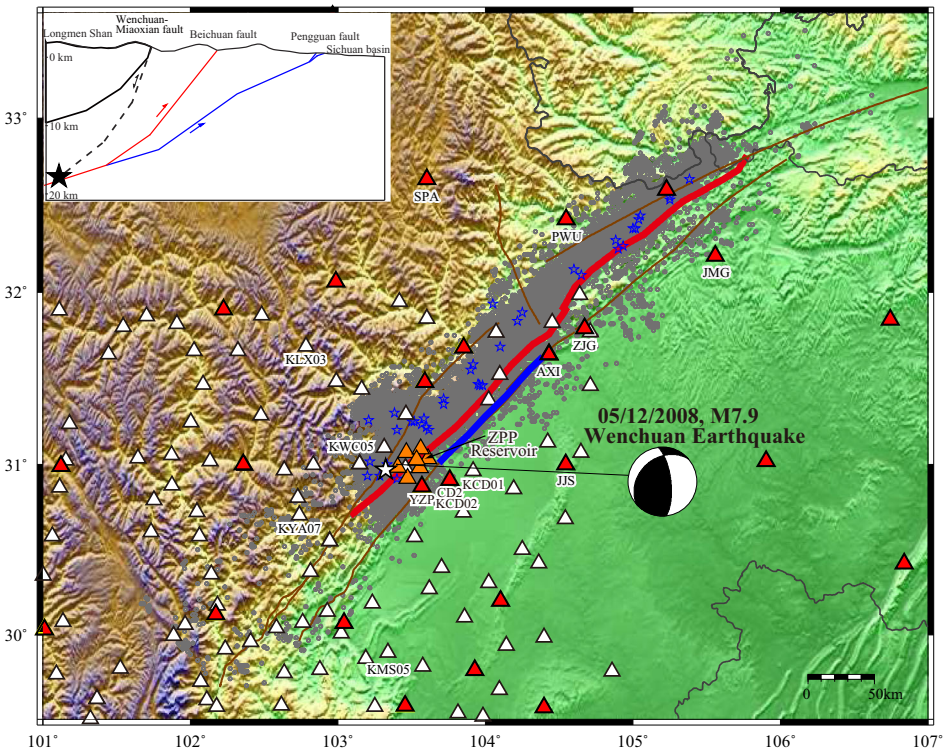


**Figure 1.** Topographic map showing the eastern margin of the Tibetan plateau and the western Sichuan basin. The brown lines show the three major faults, which constitute the Longmen Shan fault zone. Surface ruptures associated with the 2008 *M*7.9 Wenchuan earthquake along the Beichuan and Pengguan faults are marked by thick red and blue lines, respectively. The white star and the beach ball indicate the epicentre and the focal mechanism of the 2008 *M*7.9 Wenchuan earthquake. The SRSN, ZRSN and WSSA stations are shown by red, orange and white triangles, respectively. The grey circles represent the aftershocks occurring before July 2009, and the blue stars indicate those with a magnitude greater than 5.0. Inset shows a schematic cross-section of the Longmen Shan fault zone. Star indicates the hypocentre of the *M*7.9 Wenchuan earthquake.

the source (Poupinet *et al*. 1984; Niu *et al*. 2003; Schaff & Beroza 2004; Rubinstein & Beroza 2004a,b, 2005; Peng & Ben-Zion 2006; Rubinstein *et al*. 2007; Taira *et al*. 2008; Chao & Peng 2009; Zhao & Peng 2009; Cociani *et al*. 2010; Chen *et al*. 2011; Long & Wen 2012; Schaff & Kim 2012; Yu *et al*. 2013). A great number of aftershocks occurred after the *M*7.9 Wenchuan earthquake, and many of them showed very similar waveforms. In this paper we first searched for repeating aftershocks using a waveform matching technique from both event and continuous data. We found a total of 34 repeating events that occurred at 12 isolated source patches over a one-year period after the main shock, which allows us to examine the temporal evolution of the post-seismic healing process occurring inside the rupture zones of the Wenchuan earthquake. We then estimated the subsurface velocity changes by applying the coda wave interferometry (CWI) technique (Snieder 2006) to the repeating earthquake data, and found a significant velocity increase within the rupture zone in the studied one-year period.

## 2 SEISMIC DATA

We found a total of 52 889 aftershocks from the joint catalogue of the Sichuan Regional Seismic Network (SRSN) and the Zipingpu Reservoir Seismic Network (ZRSN) with a Richter magnitude between 0.1 and 6.4, which occurred over a one-year period after the earthquake. Among all the events, there are 57 aftershocks with $M \geq 5.0$ during this period (blue stars in Fig. 1). The SRSN consists of 52 broad-band stations equipped with a Guralp CMG-3ESP sensor and a Gangzhen EDAS-24IP data acquisition system. The ZRSN comprises seven closely located stations with a short-period RSFS-1A sensor and an EDAS-24L digitizer. It was designed to monitor the seismicity around the Zipingpu Reservoir and started operating in August 2004. Among the seven stations, TZP was destroyed during the Wenchuan earthquake. The average station spacing for the SRSN and ZRSN is approximately 50 and 10 km, respectively. The Western Sichuan Seismic Array (WSSA) is a temporary deployment (ChinArray 2006) between October 2006 and July 2009. It is a dense (10–30 km spacing) array with 297 broadband seismographs in western Sichuan and covers the southern two third of the fault that was activated during the 2008 Wenchuan earthquake. The sampling rate of the SRSN and ZRSN is 100 Hz while the WSSA stations are digitized at a rate of 40 samples per second.

## 3 MEASURING TEMPORAL VELOCITY CHANGES WITH REPEATING EARTHQUAKES

### 3.1 Detecting repeating earthquakes

In order to search for repeating events, we first created an event waveform dataset from continuous records according to the joint catalogue. We then filtered the raw waveform data with a 1–10 Hz bandpass filter, and further interpolated the data to a sampling interval of 0.3125 ms. As described below, we use the relative *S–P* traveltimes to determine the relative location with respect to the centroid of the cluster. Therefore the accuracy in the relative location is determined by the uncertainty in traveltime measurements, which is principle constrained by signal-to-noise ratio (SNR) of the waveform data (Cheng *et al*. 2007; Li *et al*. 2011). Based on the average

SNR, we estimated the traveltime picking error is around ∼0.3 ms, which was selected as the sampling interval for the interpolation.

After the pre-processing, we started the search for repeating events using a two-step cross-correlation (CC) method for better computational efficiency. The first step is to find out earthquakes that have similar waveforms, but not necessarily the same rupture areas. We selected the vertical channel of the waveform data recorded at the SRSN stations YZP and ZJG for computing the CC with a time window 1 s before the *P* and 5 s after the *S* arrival. We defined similar events as a group of earthquakes with a computed CC greater than 0.9 at one or more stations. After scanning the entire event waveform dataset, we obtained 2353 pairs of similar events, which were further grouped into 316 multiplets and 946 doublets. We further confirmed this selection using waveform data recorded at two other stations (BAY and LYS from ZRSN). The four stations used here are among those with the best recording quality. The CC computed with the whole *P* and *S* wave window (hereafter referred to as whole-window CC) could be dominated by the main *P* and *S* arrivals, and it has been known that similar aftershocks with rupture area displaced from each other can generate very similar *P* and *S* waveforms (Cheng *et al*. 2007). The coda waves of displaced similar events can be quite different due to the slightly difference in ray path in the source region. Therefore we further computed the CCs of the *P* and *S* coda (coda CCS) with a 0.5 s long running time window, and used them in the final selection of repeating earthquakes. This is done collectively with the relocation process described below. Only 28 events were left with this scrutiny, which are located at 12 different clusters.

Seismic event detection is generally performed by the simple and fast short-term-average/long-term-average (STA/LTA) criterion using continuous records of a seismic network (e.g. Allen 1978). It is well known that a particular network can only detect earthquakes above certain magnitude. The completeness magnitude ($M_c$) is the magnitude above which all events are reported. Seismic events with a magnitude smaller than $M_c$ can be easily missed due to the low SNR of the corresponding records. The regular STA/LTA detection becomes even more vulnerable in the case of detecting and locating aftershocks, as many of the aftershocks can occur simultaneously at different parts of the rupture area, which results in complicated recordings due to waveform interference. The complexity requires great scrutiny in signal association (e.g. Peng & Zhao 2009; Schaff 2010). Therefore many aftershock events might have been missed and excluded in a routine catalogue determined by the STA/LTA detection algorithm.

In order to obtain a complete event catalogue for the identified 12 repeating clusters, we employed a template (pattern) matching technique to scan the continuous records of SRSN stations, YZP and ZJG, together with two ZRSN stations, BAY and LYS. We used all the 28 events in the 12 clusters as the templates to search for missing events in each cluster. The template signal window is usually a few to tens of seconds long and contains both the main *P* and *S* arrivals. When the CC computed from a certain time window reaches to a critical value (0.9) at the three stations in the southwestern segment (YZP, BAY and LYS) and one station (ZJG) in the northeastern segment, we consider it as detection of one repeating event. We were able to detect all the 28 known events from this template matching technique. In addition, we found additional six events, which were not listed in the joint event catalogue. We further estimated their Richter magnitude using corrections of the instrument response and attenuation structure given by the SRSN.

In order to further confirm whether the 34 earthquakes in the 12 clusters share rupture areas, that is, repeating events, we used *S–P* differential traveltime to estimate their relative locations. For each cluster, we first collected all the seismograms recorded at each station, and aligned them along the *P* arrivals using a CC method. We further normalized the *P* waveforms and averaged them to generate a reference *P* wavelet. We repeated the same procedure for *S* arrival to generate a reference *S* wavelet. We further computed the *S–P* differential traveltime from these two reference wavelets, which can be considered as the *S–P* differential traveltime from a virtual earthquake occurring at the centroid of the cluster. Here we refer it to as the reference *S–P* time. Next, we cross-correlated each *P* and *S* waves with these two template wavelets to obtain the relative *S–P* differential traveltimes with respect to the reference *S–P* time. We then used these relative differential traveltimes to constrain the relative location with respect to the centroid for each earthquake in a cluster. Compared to the individual traces, the stacked *P* and *S* waveforms possess higher SNR, leading to more accurate measurements of *S–P* differential traveltimes.

We applied the fine relocation method (Got *et al*. 1994; Cheng *et al*. 2007) to obtain the relative locations between each event and the sequence centroid. We further used a 3-D grid searching method (Cheng *et al*. 2007) to estimate the uncertainties in the relative locations. For each grid, we computed the RMS residual *S–P* time. By comparing the RMS residual times with the uncertainties in the *S–P* traveltime measurements (∼0.3 ms), we can obtain the error ellipse along the fault plane. We further assumed a circular rupture area for each earthquake and computed the rupture radius from its magnitude under a given stress drop of 5 MPa (Li *et al*. 2011). Fig. 2 shows the distribution of the relocated events in all the sequences, which suggests that all the events in each sequence are literally co-located. In Fig. 2, the horizontal and vertical lines represent the two axes of the error ellipses, and the shaded circles are the reference ones, which are calculated from the average magnitudes of each sequence.

### 3.2 Measuring temporal velocity changes using CWI

Following Niu *et al*. (2003), we first aligned the bandpass filtered (1–10 Hz) seismograms at each station recorded from each repeating sequence to the *P* arrival by using the CC technique. We then computed the running CCs between the first seismogram and each subsequent seismogram within a 0.5 s moving time window. At each time window starting at $t$, we obtained the lag time $\tau(t)$ when the CC reaches its maximum, $C_m(t)$. The decorrelation index $D(t)$ is defined as $1 - C_m(t)$.The lag time function $\tau(t)$ can be considered as the mean traveltime perturbation of the lag times, $\tau_i$, associated with the arrivals of individual scatterers in the time window starting at $t$, while $D(t)$ can be linked to the variance of the travel time perturbations, $\sigma_\tau{}^2(t)$, by the equation $D(t) = \frac{1}{2}\omega^2\sigma_\tau{}^2(t)$ (Snieder 2006), where $\omega$ is the characteristic angular frequency of the scattered waves.

Eight examples of the time lag $\tau$ and decorrelation index $D(t)$ measured at SRSN stations, YZP, ZJG, AXI, CD2, and one ZRSN station, ZDZ, are shown in Fig. 3; both are plotted as a function of the elapse time, $t$. The measured time delays usually show some linear trend after the *S* arrivals, and the decorrelation index is generally of low amplitude across most of the *S*-coda window. Both the lag time and decorrelation functions show large spikes. Spikes on the lag and decorrelation functions are likely caused by perturbations in the scatterer location or by a velocity changes around the scatterers (Niu *et al*. 2003). Using the lag times of a spike recorded by the dense HRSN array, Niu *et al*. (2003) were able to locate a 'moving'

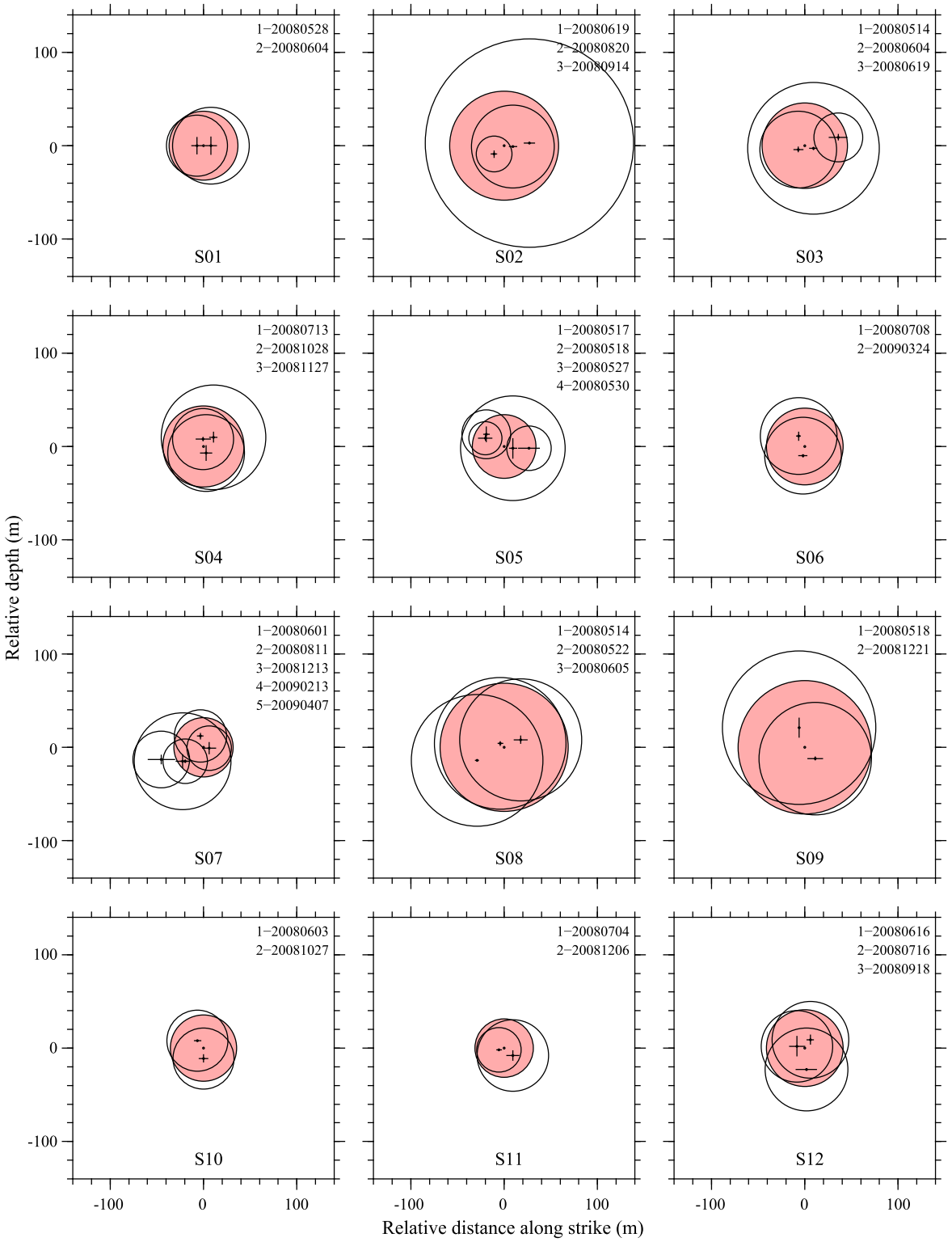


**Figure 2.** Map view of the relative locations of member events with respect to the cluster centroid for all the 12 sequences. The shaded region in each plot represents the rupture area of a virtual reference event with the mean magnitude of the cluster located at the centroid. The two black lines at the centre of each circle indicate the two axes of the error ellipse. Note that all the events in each sequence overlap each other. Event occurrence date is indicated in each panel.

scatterer within the San Andreas fault zone at a depth of ∼3 km, which was interpreted to be the result of stress-induced redistribution of fluids in fluid-filled fractures. Here the station coverage is, however, not dense enough for performing migration to locate the corresponding scatterers of the spikes. Therefore we decided to focus on bulk velocity changes in this study.

It has been shown that when and only when there is a change in the background velocity field, $\tau$ and $t$ exhibit a linear relationship

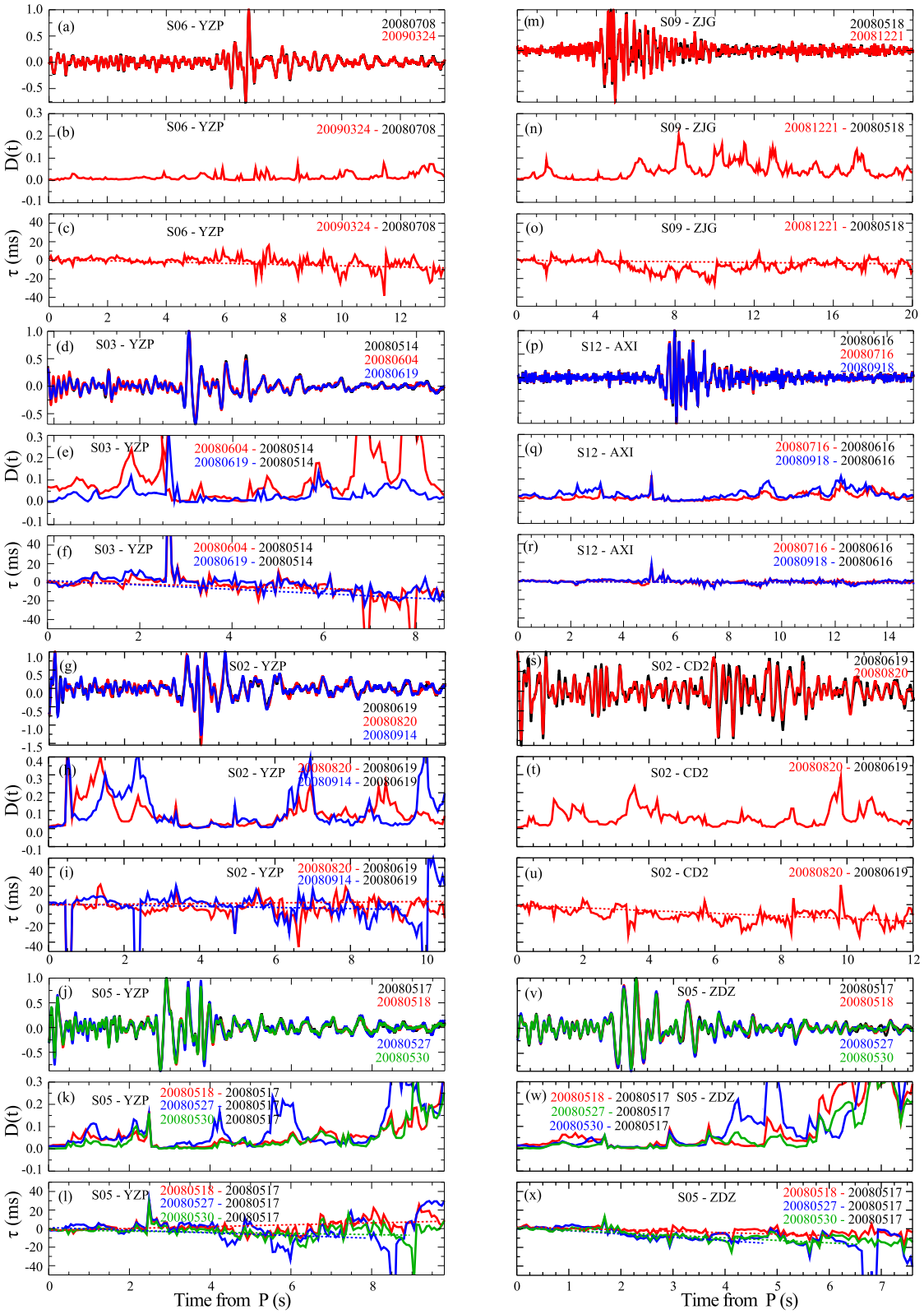


**Figure 3.** (a) Overlap of the vertical-component seismograms recorded at YZP from the repeating earthquakes in the S06, plotted in different colours that are labelled in the panel. The calculated decorrelation index, $D(t)$, and lag time function, $\tau(t)$, are shown in the (b) and (c), respectively. The colour scheme used in plotting $D(t)$ and $\tau(t)$ is similar to (a), and is also labelled in the panel. The dotted line in (c) shows the linear trend computed from linear regression. (d–f) The same as panels (a)–(c), but for YZP from S03. (g–i) The same as panels (a)–(c), but for YZP from S02. (j–l) The same as panels (a)–(c), but for YZP from S05. (m–o) The same as panels (a)–(c), but for ZJG from S09. (p–r) The same as panels (a)–(c), but for AXI from S12. (s–u) the same as (a)–(c), but for CD2 from S02. (v–x) The same as panels (a)–(c), but for ZDZ from S05.

**Table 1.** Information of the 12 repeating earthquake sequences.

| ID | N§ | Sequence centroid location | | | $M_L$ | D¶ (days) |
|---|---|---|---|---|---|---|
| | | Lon. (°) | Lat. (°) | Dep. (km) | | |
| S01 | 2 | 103.3750 | 30.8583 | 4.7 | 1.8–2.1 | 7 |
| S02 | 3 | 103.3417 | 30.9752 | 7.2 | 1.1–3.4 | 87 |
| S03 | 3 | 103.4333 | 30.9920 | 13.4 | 1.5–2.8 | 36 |
| S04 | 3 | 103.1834 | 31.0122 | 7.0 | 1.8–2.5 | 137 |
| S05 | 4 | 103.4167 | 31.0167 | 10.0 | 1.0–2.5 | 13 |
| S06 | 2 | 103.4000 | 31.2583 | 2.7 | 2.1–2.1 | 259 |
| S07 | 5 | 103.5749 | 31.2917 | 3.9 | 1.4–2.4 | 310 |
| S08 | 3 | 103.3825 | 31.3500 | 13.3 | 2.7–2.8 | 22 |
| S09 | 2 | 104.4951 | 32.0330 | 13.0 | 2.6–3.0 | 217 |
| S10 | 2 | 104.3330 | 31.9000 | 8.8 | 1.8–1.8 | 146 |
| S11 | 2 | 104.3085 | 31.9330 | 10.4 | 1.4–2.0 | 155 |
| S12 | 3 | 104.4560 | 31.9945 | 12.9 | 2.0–2.1 | 94 |

N§: number of earthquakes in one sequence; D¶: sequence duration.

(e.g. Niu *et al*. 2003). The fractional change of the background velocity, $\delta v/v$, equals to the negative slope of the linear trend, $-\tau/t$ (Fig. 3). In order to estimate the linear trend in a time lag function, we employed the linear regression method (Press *et al*. 1992) that minimizes the chi-square merit function, which is $\chi^2(a,b) = \Sigma[(\tau(t) - a - bt)/\sigma(t)]^2$, where $b$ and $a$ are the slope and intercept, respectively. $\sigma(t)$ is the uncertainty at time $t$, and is determined by its SNR. In the linear regression, we only used the lag time with a corresponding decorrelation index being less than 0.3.

## 4 RESULTS AND DISCUSSION

### 4.1 Spatial and temporal distribution of the repeating earthquakes

As mentioned in the previous section, we employed a strict scrutiny in identifying repeating earthquakes, which led to the detection of 34 repeating earthquakes spreading over 12 different clusters (Table 1). In Fig. 4, we plotted the time evolution of the 12 repeating sequences, in which, the grey symbols indicate the 6 additional events detected from continuous records. The size of the symbols is proportional to earthquake magnitude, which varies from 1.0 to 3.4. Each sequence contains 2–5 events occurring from 2008 May 14 through 2009 April 7. It appears that the repeating events occurring immediately after the main shock have shorter recurrence intervals and larger magnitude variations.

Among the 12 clusters, 8 are located in the initial rupture zone of the 2008 Wenchuan earthquake in the southwest, and 4 are found in the northeastern section of the rupture zone (Fig. 5). They occurred in a depth range from 2.7 to 13.4 km (Fig. 5 inset). For each cluster we determined its centroid by using the *P*- and *S*-wave traveltimes of the containing earthquakes with a revised double difference relocation technique (Li *et al*. 2011). Since there is a large velocity contrast between the Sichuan basin and the Tibetan plateau located in the eastern and western sides of the Longmen Shan fault zone, we used two different 1-D velocity models when we applied the HYPODD package (Waldhauser & Ellsworth 2000) in the centroid relocation. We also relocated the 4 aftershocks shown in Fig. 5 using the Hypo2000 method (Klein 2002). Based on the their 3-D location, we inferred that the S06 and S04 clusters could have occurred on the Wenchuan-Maoxian fault, where no surface rupture was observed during the main shock (Xu *et al*. 2009).

### 4.2 Velocity changes and fault-zone healing across the rupture area

We used the first event as the reference for computing the lag time, which left 22 measurements of the velocity changes. Details on the measured velocity changes are listed in Table 2. Fig. 6(a) shows the observed bulk velocity changes from all the 12 clusters, and Fig. 7 shows the changes observed by each cluster. In both case, the measured velocity changes are shown at the occurrence time of the subsequent events. The geographic location of the stations used in plotting Figs 6(a) and 7 are shown in both Fig. 1. These stations are taken from all the three networks. In Fig. 6(a), it appears that measurements from two clusters, S02 and S05, are featured by large uncertainties at each station, significant variations among stations, and strong perturbations among subsequent events. The large uncertainties may be related to the large variations in event

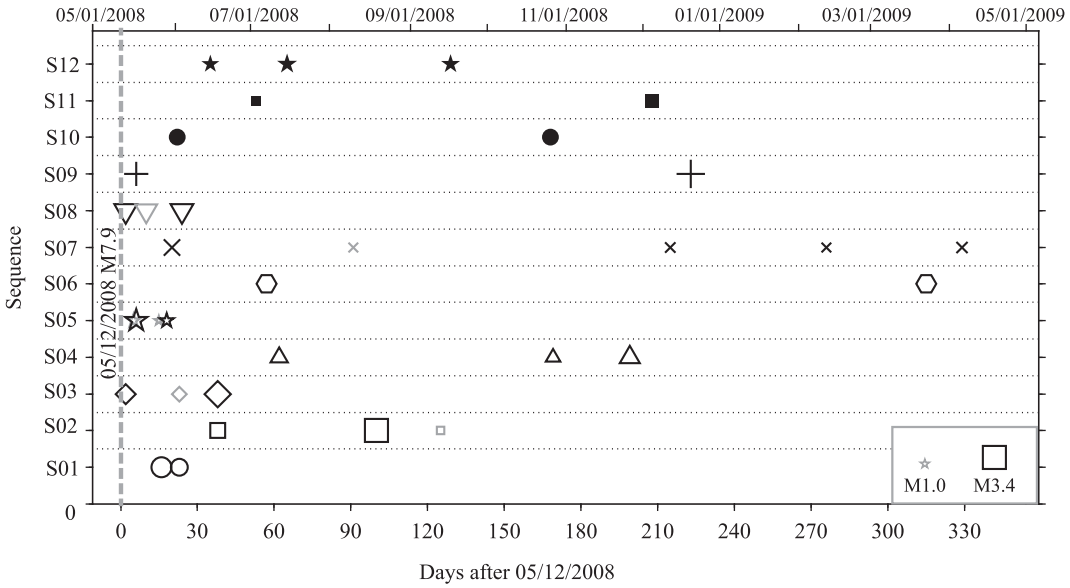


**Figure 4.** Recurrence times of all the 34 earthquakes that make up the 12 clusters. Different symbols were used to indicate different sequences. The grey symbols represent the missing members from the joint catalogue. Symbol size is proportional to event magnitude.

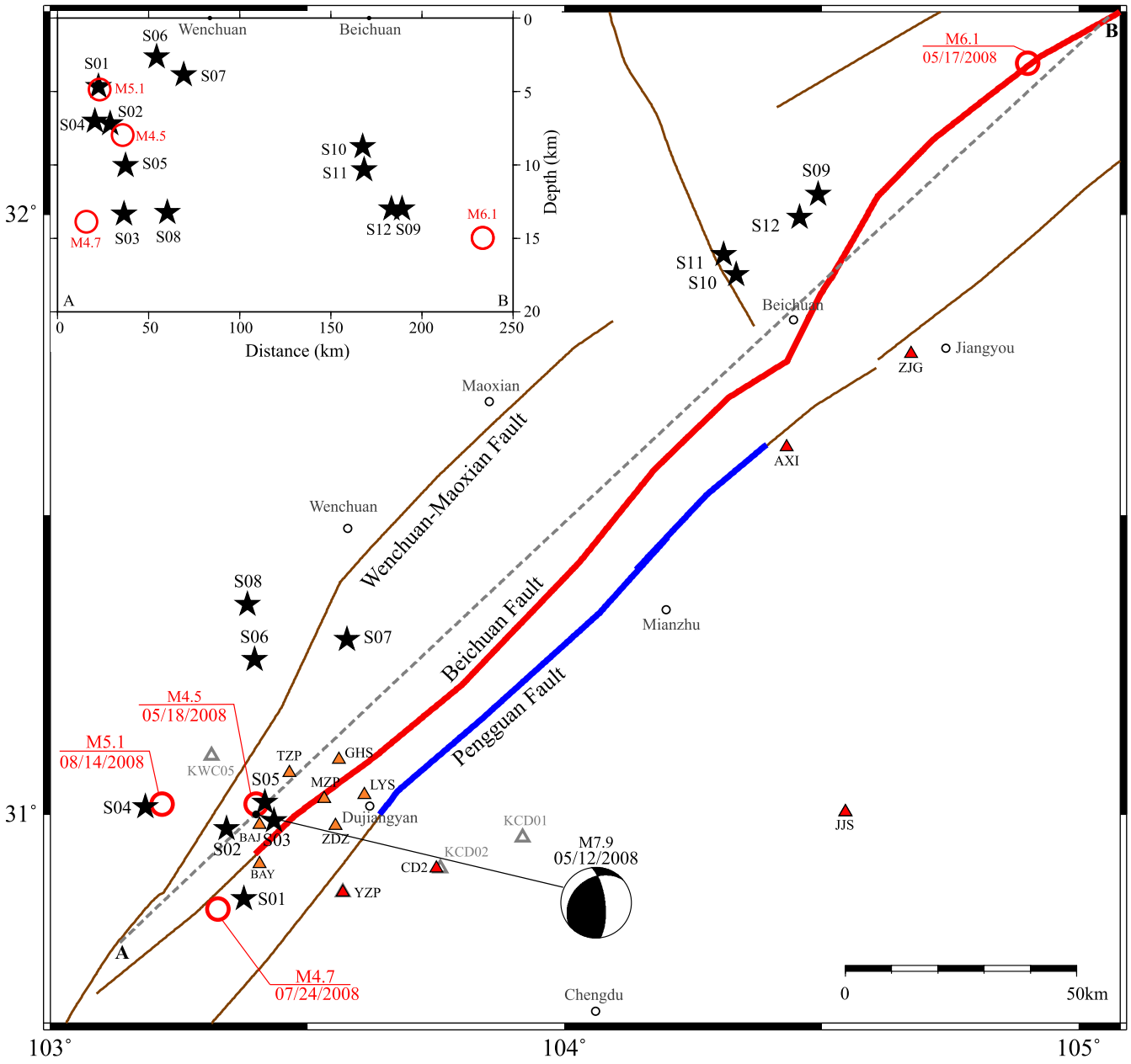


**Figure 5.** Map view of the repeating earthquake sequences (black stars) and stations used in calculating velocity changes (triangles). Stations are plotted similarly to Fig. 1. The locations of four aftershocks with $M \geq 4.5$ discussed in the text are shown in red circles. Surface ruptures associated with the 2008 *M*7.9 Wenchuan earthquake along Beichuan and Pengguan faults are marked by thick red and blue lines, respectively. Inset shows the depth cross-section view of repeating earthquake sequences (black stars) along the dashed line AB in the map.

size of these two clusters, which can reduce the overall waveform similarity of the clusters, leading to large measurement errors.

Overall, velocity changes estimated from the eight clusters (S01–S08) located in the initial rupture area of the Wenchuan earthquake in the southwest are significant, while those observed from the four northeastern sequences (S09–S11) are almost negligible (Fig. 8). Among the 12 clusters, the doublet S06 and the quasi-periodic multiplet S07 possess the longest sequence duration of 259 and 310 d, respectively (Tables 1 and 2, Figs 7f and g).Velocity changes estimated from these two clusters are consistent across all the stations, and exhibit a stable increase of ∼0.1 per cent, which implies that the most velocity recovery is achieved shortly after the main shock. In contrast, velocity changes estimated from the northeastern four sequences are in the range between 0.019 ± 0.011 per cent and 0.056 ± 0.026 per cent (Table 2, Figs 7 and 8), which are roughly an order of magnitude smaller than those observed in the southwest (Fig. 5). This suggests that no significant post-seismic velocity change occurred around the northern section of the Beichuan fault, although a maximum coseismic slip of 6.5 ± 0.5 m was observed in the area (Xu *et al*. 2009).

The distinct contrast in medium velocity change observed between the southwestern and northeastern sections of the rupture zone may suggest that the two sections are undergoing different healing processes, or they had different medium damage during the main rupture. Many studies (e.g. Ji *et al*. 2008; Hao *et al*. 2009; Shen *et al*. 2009; Xu *et al*. 2009; Zhang *et al*. 2009; Zhao *et al*.

**Table 2.** Earthquake origin time, magnitude and measured velocity changes.

| EID | SID | Origin time | | $M_L$ | N§ | $\delta v_{max}/v$ (%) | $\delta v_{min}/v$ (%) |
|---|---|---|---|---|---|---|---|
| | | Date | Time | | | | |
| E01 | S01 | 05/28/2008 | 23:03:03.8 | 2.1 | 5 | — | — |
| E02 | S01 | 06/04/2008 | 23:35:01.6 | 1.8 | 5 | $0.126 \pm 0.005$ | $0.047 \pm 0.017$ |
| E03 | S02 | 06/19/2008 | 20:50:54.2 | 2.2 | 4 | — | — |
| E04¶ | S02 | 08/20/2008 | 19:34:56.9 | 3.4 | 4 | $0.100 \pm 0.016$ | $0.100 \pm 0.016$ |
| | | | | | | $-0.116 \pm 0.024$ | $-0.077 \pm 0.046$ |
| E05 | S02 | 09/14/2008 | 13:38:52.4 | 1.1 | 3 | $0.265 \pm 0.158$ | $0.038 \pm 0.024$ |
| E06 | S03 | 05/14/2008 | 16:44:06.1 | 2.1 | 7 | — | — |
| E07 | S03 | 06/04/2008 | 17:53:10.0 | 1.5 | 2 | $0.135 \pm 0.080$ | $0.135 \pm 0.061$ |
| E08 | S03 | 06/19/2008 | 15:11:03.0 | 2.8 | 6 | $0.273 \pm 0.051$ | $0.036 \pm 0.019$ |
| E09 | S04 | 07/13/2008 | 01:55:31.9 | 2.1 | 7 | — | — |
| E10 | S04 | 10/28/2008 | 16:19:34.4 | 1.8 | 5 | $0.315 \pm 0.027$ | $0.071 \pm 0.015$ |
| E11 | S04 | 11/27/2008 | 12:03:26.2 | 2.5 | 7 | $0.217 \pm 0.099$ | $0.073 \pm 0.010$ |
| E12 | S05 | 05/17/2008 | 09:12:00.4 | 1.4 | 4 | — | — |
| E13¶ | S05 | 05/18/2008 | 16:34:11.7 | 2.5 | 3 | $0.104 \pm 0.018$ | $0.026 \pm 0.014$ |
| | | | | | | $-0.102 \pm 0.021$ | $-0.102 \pm 0.021$ |
| E14 | S05 | 05/27/2008 | 04:40:02.8 | 1.0 | 3 | $0.294 \pm 0.091$ | $0.172 \pm 0.036$ |
| E15 | S05 | 05/30/2008 | 09:26:49.0 | 1.5 | 3 | $0.217 \pm 0.020$ | $0.036 \pm 0.031$ |
| E16 | S06 | 07/08/2008 | 10:22:55.8 | 2.1 | 6 | — | — |
| E17 | S06 | 03/24/2009 | 05:10:57.7 | 2.1 | 6 | $0.154 \pm 0.011$ | $0.065 \pm 0.043$ |
| E18 | S07 | 06/01/2008 | 22:56:19.2 | 2.4 | 6 | — | — |
| E19 | S07 | 08/11/2008 | 22:07:31.5 | 1.4 | 5 | $0.206 \pm 0.005$ | $0.022 \pm 0.011$ |
| E20 | S07 | 12/13/2008 | 15:12:43.6 | 1.6 | 2 | $0.142 \pm 0.019$ | $0.139 \pm 0.026$ |
| E21 | S07 | 02/13/2009 | 18:42:02.5 | 1.4 | 3 | $0.155 \pm 0.013$ | $0.107 \pm 0.017$ |
| E22 | S07 | 04/07/2009 | 20:24:38.7 | 1.7 | 2 | $0.149 \pm 0.040$ | $0.105 \pm 0.018$ |
| E23 | S08 | 05/14/2008 | 18:59:00.2 | 2.8 | 9 | — | — |
| E24 | S08 | 05/22/2008 | 06:19:11.4 | 2.7 | 7 | $0.084 \pm 0.010$ | $0.020 \pm 0.008$ |
| E25 | S08 | 06/05/2008 | 21:20:14.4 | 2.8 | 6 | $0.093 \pm 0.013$ | $0.008 \pm 0.005$ |
| E26 | S09 | 05/18/2008 | 14:39:54.9 | 2.6 | 6 | — | — |
| E27 | S09 | 12/21/2008 | 12:39:11.5 | 3.0 | 6 | $0.048 \pm 0.013$ | $0.011 \pm 0.002$ |
| E28 | S10 | 06/03/2008 | 14:39:35.2 | 1.8 | 4 | — | — |
| E29 | S10 | 10/27/2008 | 18:07:08.7 | 1.8 | 4 | $0.025 \pm 0.014$ | $0.006 \pm 0.001$ |
| E30 | S11 | 07/04/2008 | 20:39:18.8 | 1.4 | 3 | — | — |
| E31 | S11 | 12/06/2008 | 19:09:04.1 | 2.0 | 3 | $0.056 \pm 0.026$ | $0.020 \pm 0.012$ |
| E32 | S12 | 06/16/2008 | 14:10:36.4 | 2.0 | 3 | — | — |
| E33 | S12 | 07/16/2008 | 06:37:35.1 | 2.2 | 3 | $0.019 \pm 0.011$ | $0.008 \pm 0.003$ |
| E34 | S12 | 09/18/2008 | 22:36:03.9 | 2.1 | 3 | $0.052 \pm 0.024$ | $0.005 \pm 0.002$ |

N§: number of stations recorded; ¶: negative/positive velocity changes coexist.

2010) suggested that the 2008 Wenchuan earthquake involved complicated and multiple ruptures, changing from thrusting dominated in the southwest to a right lateral strike slip motion in the northeast. We speculate that the observed contrast in velocity change here might be partly related to this rupture difference. The thrust rupture in the southwest might produce a wide damage zone, involving all the major faults in the Longmen Shan range front, including the Wenchuan-Maoxian fault, the Beichuan fault, and the Pengguan fault (Xu *et al*. 2009). On the other hand, the strike-slip rupture in the northeast is likely to have occurred only along the Beichuan fault, resulting in a damage zone less wide than the one in the southwest (Xu *et al*. 2009). One argument for this is that the aftershock seismicity appears to be more widely distributed in the southwest than it is in the northeast (Fig. 1). As mentioned in the previous section, a localized velocity change is manifested by a spike, not a linear trend, in the computed lag time function, $\tau$ ($t$), and thereby results in a negligible $\delta v/v$.

In addition to the S06 and S07 clusters in the southwest, four other sequences (S01, S03, S04 and S08) also exhibit a systematical increase of the background velocity at all the stations. The average velocity increase from the above 6 sequences ranges between 0.1 per cent and 0.3 per cent, suggesting that fault healing has been continuously happening within the southwestern section of the rupture zone of the $M$7.9 earthquake at the post-seismic stage. Measurements from two other clusters in the southwest, S02 and S05, however, showed some fluctuation about this post-seismic healing. For the S02 cluster that consists of three events, three stations located in the thrust front, YZP, BAY and LYS, show a slightly positive linear trend in the lag time function $\tau(t)$ (red line in Fig. 3i), indicative of a velocity drop between the first and second events, which occurred on 2008 June 19 and 2008 August 20, respectively (Figs 6b and 7b). The velocity drop measured at the three stations varies from $0.077 \pm 0.046$ per cent to $0.116 \pm 0.024$ per cent (Table 2). The CD2 station located inside the Sichuan basin, however, showed an increase of 0.1 per cent over the same period (Figs 3u, 6b and 7b). We checked the aftershock seismicity in the source region and found two large aftershocks; one $M$4.7 and another $M$5.1 occurred near the S02 cluster on 2008 July 24 and 2008 August 14, respectively. The $M$5.1 aftershock occurred within the thrust front at a depth slightly shallower than the S02 cluster (Fig. 5). It is only ~25 km away from the S02 cluster (Fig. 5), so close that it could cause significant damage to the front of Longmen Shan range. The damage could have resulted in a velocity decrease within the wedge beneath the front, which was recorded by the stations above

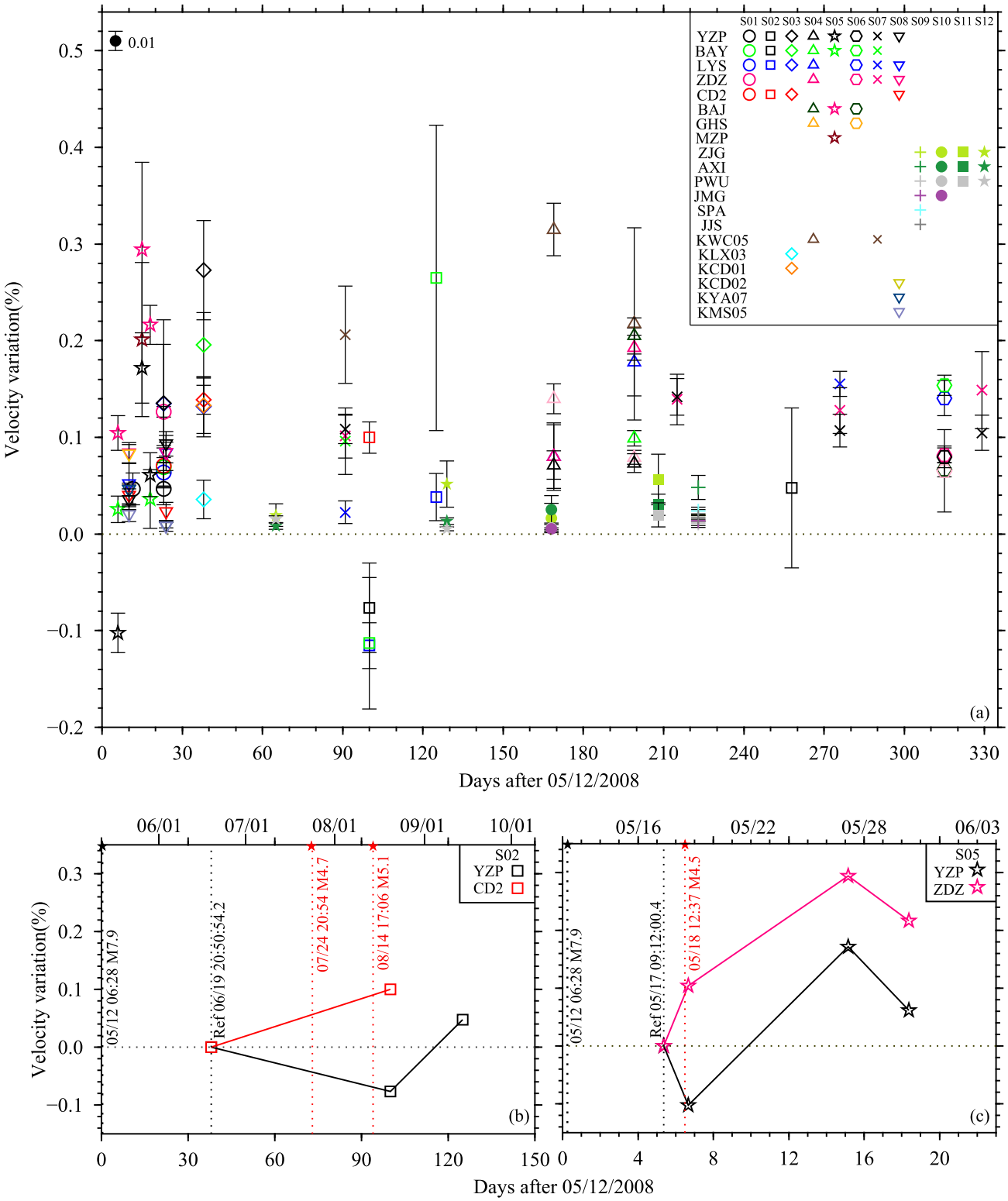


**Figure 6.** (a) Velocity changes estimated from the *S*-wave coda of all the earthquakes in the 12 sequences are plotted as a function of the occurrence time of the subsequent events. Symbols correspond to those used in Fig. 4 for each sequence. Different colours represent different stations. (b) Temporal evolution of S02 shows a clear coseismic drop and rapid recovery associated with the aftershocks. (c) The same as (b) but for S05.

(BAY and LYS) and nearby (YZP). On the other hand, it probably has very limited effect on the crust beneath the Sichuan basin located in the other side of the Longmen Shan fault system, and thereby was not shown at the CD2 station (Fig. 5). The *M*5.1 aftershock might have also affected the repeating earthquakes within the S02 sequence, which has the largest degree of variability in magnitude (*M*1.1–*M*3.4). We noticed that the sequence had a sudden increase of magnitude shortly after the *M*5.1 aftershock, followed

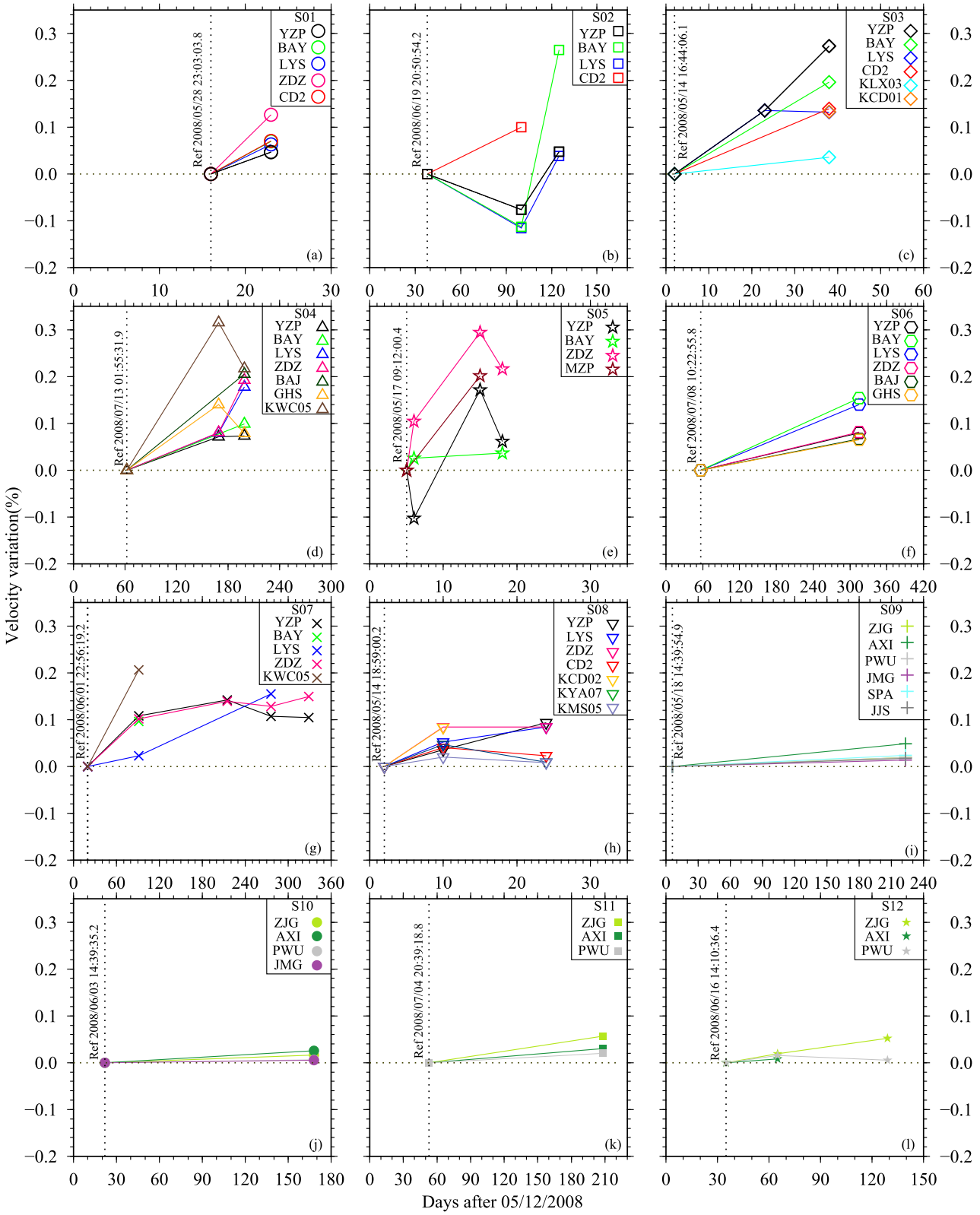


**Figure 7.** The temporal velocity changes estimated from the *S*-wave coda of repeating earthquakes in each sequence at different stations. Symbols correspond to those used in Fig. 4 for each sequence. Different colours represent different stations listed in Fig. 6.

by a magnitude drop of the subsequent event (Figs 4, 5, 6b and 7b).

From the S05 cluster, we also observed a velocity drop of 0.102 per cent at the YZP station between the first and second events occurring on 2008 May 17 and 18, respectively (Figs 3l, 6c and 7e). There is an *M*6.1 aftershock occurring in this period, but is expected to have a limited effect on the S05 source region as it is located in the northeastern section of the Beichuan fault, and is more than

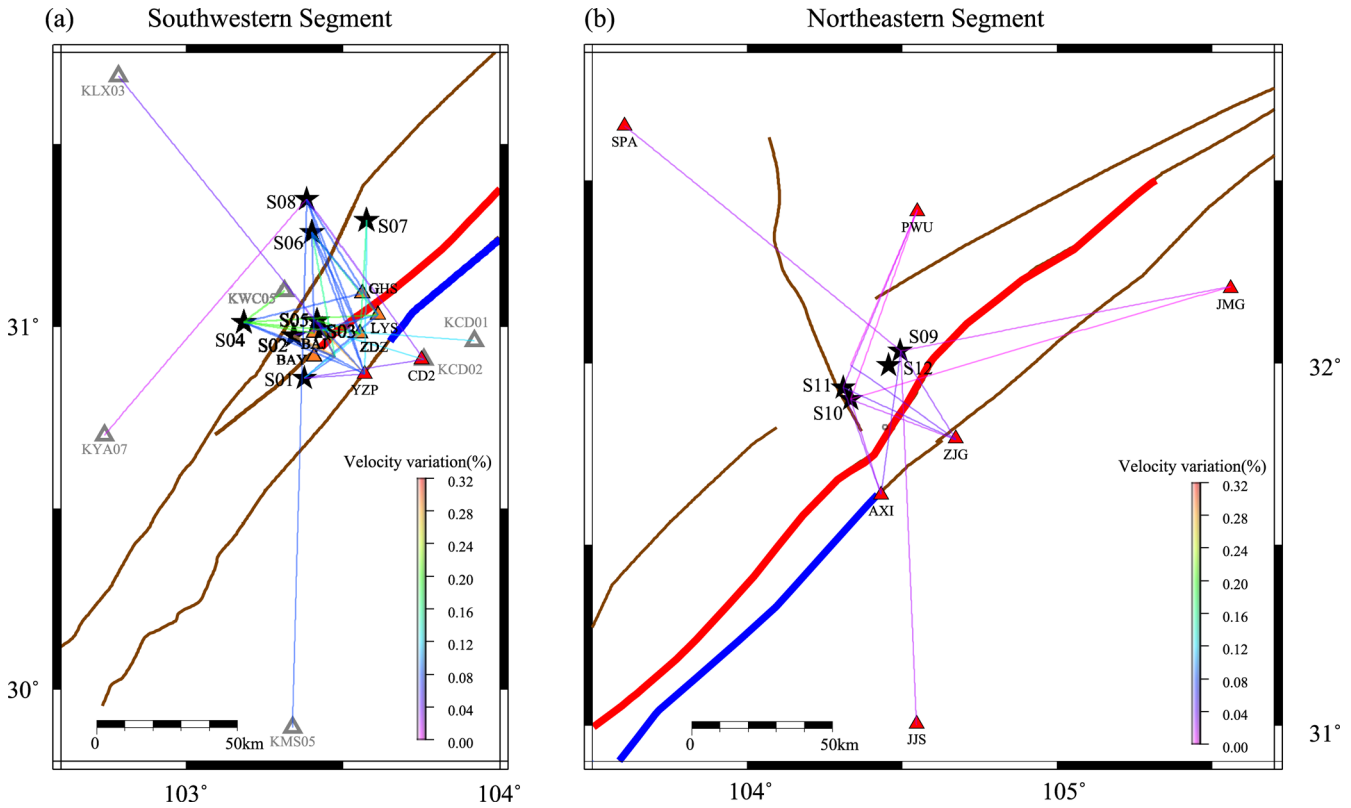


**Figure 8.** Maps showing the eight clusters in the southwestern section (a) and the four clusters in the northeastern section (b). The observed velocity changes between the first and last earthquakes in each sequence are plotted along the ray paths between clusters and the stations. The amplitude of the changes is indicated by colour. Note the large difference in the amplitude of velocity changes between (a) and (b), which are shown mainly in blue and purple, respectively. Thick red and blue lines indicate the surface ruptures along the Beichuan and Pengguan faults, respectively.

200 km away from the S05 cluster (Fig. 5). On the other hand, there is a *M* 4.5 aftershock occurring only a few kilometres away from the S05 cluster on 2008 May 18 (Fig. 5), which should have an impact on the medium in the S05 source region, as well as the occurrence of repeating events in the cluster, including both size and recurrence interval. It is, however, unclear to us why the two ZRSN stations, BAY and ZDZ, showed a negative linear trend in the lag time plot (Fig. 3x), leading to estimates of a velocity increase of $0.026 \pm 0.014$ per cent and $0.104 \pm 0.018$ per cent in the same period (Table 2, Figs 6 and 7e). Strong shaking and large damage occurred around the Zipingpu Reservoir during the *M*7.9 Wenchuan earthquake, therefore post-seismic healing may still have played a major role even though the *M*4.5 aftershock could have affected the S05 source region substantially. In contrast, the surface area around the YZP station is less damaged, so velocity changes along the ray path from the cluster to the station are mainly disturbed by the *M*4.5 aftershock.

As mentioned above, S05 is another sequence with large magnitude variation and irregular short recurrence time. The measured velocity changes from this cluster showed large fluctuations over a 13 d period between 2008 May 17 and 30 (Figs 6a, c and 7e). The estimated velocity changes between the first and three subsequent events are $0.104 \pm 0.018$ per cent, $0.294 \pm 0.091$ per cent, and $0.217 \pm 0.020$ per cent at the ZRSN station ZDZ, and $-0.102 \pm 0.021$ per cent, $0.172 \pm 0.036$ per cent and $0.061 \pm 0.023$ per cent at the SRSN station YZP. It is difficult to explain these large perturbations with the stable healing process. Rather, it must involve multiple processes such as effects from nearby large aftershocks, as well as changes in barometric pressure loading (e.g. Silver *et al*. 2007; Niu *et al*. 2008; Chen *et al*. 2014). Changes in water level within the Zipingpu Reservoir could also lead to temporal variations of the subsurface stress field, resulting in short-term changes in subsurface velocity.

## 5 CONCLUSIONS

We employed a template matching method to analyse the event and continuous waveform data recorded by three types of seismic networks in the 2008 Wenchuan earthquake area to identify repeating earthquakes in order to investigate the post-seismic velocity changes within the rupture zone of the main shock. We identified a total 34 repeating earthquakes spreading over 12 separated clusters from the one-year aftershock sequence of the *M*7.9 earthquake. We further used a grid search technique to determine the relative location of the repeating events in each sequence to ensure their rupture areas overlap each other. We applied the coda wave interferometry technique to the *S* coda of the repeating earthquakes to estimate velocity changes between the first and subsequent events in each cluster. Our results suggest the following conclusions: (1) There is a significant difference in subsurface velocity change and post-seismic healing between the southwestern and northeastern parts of the rupture zone, which are characterized by thrust and strike slip motion, respectively, during the main rupture. Large velocity increases (~0.1–0.3 per cent) are observed in the southwest where the main rupture was initiated, while almost no significant velocity change is found in the northeast Beichuan area. (2) The post-seismic velocity healing could be temporally interrupted by

significant aftershocks, which can cause velocity drops around the source regions of the repeating sequences. (3) Short-term perturbation in velocity changes are also present from one of the cluster data, suggesting that healing of the weakened Longmen Shan thrust front in the Wenchuan area can be easily affected by various processes with different time scales, such as aftershocks, barometric pressure loading, reservoir water level changes, etc.

## ACKNOWLEDGEMENTS

We thank the Sichuan Seismic Network and China Seismic Array Data Management Center at Institute of Geophysics, China Earthquake Administration for providing the data. We also thank Dr Amir Allam and another anonymous reviewer for their constructive comments and suggestions, which significantly improved the quality of this paper. This study has been supported by research grants from NSFC (41474031, 41274099 and 41130316), CEA (2015IES0407 and 2015IES010203) and NSF grant 1251667. Maps were plotted using GMT software (Wessel & Smith 1998).

## REFERENCES

Allen, R., 1978. Automatic earthquake recognition and timing from single trace, *Bull. seism. Soc. Am.,* **68,** 1521–1532.

Chao, K. & Peng, Z.G., 2009. Temporal changes of seismic velocity and anisotropy in the shallow crust induced by the 1999 October 22 M 6.4 Chia-Yi, Taiwan earthquake, *Geophys. J. Int.,* **179,** 1800–1816.

Chen, J.H., Froment, B., Liu, Q.Y. & Campillo, M., 2010. Distribution of seismic wave speed changes associated with the 12 May 2008 $M_w$ 7.9 Wenchuan earthquake, *Geophys. Res. Lett.,* **37,** L18302, doi:10.1029/2010GL044582.

Chen, K.H., Furumura, T., Rubinstein, J. & Rau, R.J., 2011. Observations of changes in waveform character induced by the 1999 $M_w$ 7.6 Chi-Chi earthquake, *Geophys. Res. Lett.,* **38,** L23302, doi:10.1029/2011GL049841.

Chen, H.C., Ge, H.K. & Niu, F., 2014. Semiannual velocity variations around the 2008 $M_w$ 7.9 Wenchuan Earthquake fault zone revealed by ambient noise and ACROSS active source data, *Earthq. Sci.,* **27**(5), 529–540.

Cheng, X., Niu, F., Silver, P.G., Horiuchi, S., Takai, K., Iio, Y. & Ito, H., 2007. Similar microearthquakes observed in western Nagano, Japan, and implications for rupture mechanics, *J. geophys. Res.,* **112,** B04306, doi:10.1029/2006JB004416.

Cheng, X., Niu, F. & Wang, B.S., 2010. Coseismic velocity change in the rupture zone of the 2008 $M_w$ 7.9 Wenchuan earthquake observed from ambient seismic noise, *Bull. seism. Soc. Am.,* **100**(5B), 2539–2550.

ChinArray, 2006. *China Seismic Array Waveform Data,* China Earthquake Administration, doi:10.12001/ChinArray.Data.

Cociani, L., Bean, C.J., Lyon-Caen, H., Pacchiani, F. & Deschamps, A., 2010. Coseismic velocity variations caused by static stress changes associated with the 2001$M_w$ 4.3 Agios Ioanis earthquake in the Gulf of Corinth, Greece, *J. geophys. Res.,* **115,** doi:10.1029/2009JB006859.

Froment, B., Campillo, M., Chen, J.H. & Liu, Q.Y., 2013. Deformation at depth associated with the May 12, 2008 $M_w$ 7.9 Wenchuan earthquake from seismic ambient noise monitoring, *Geophys. Res. Lett.,* **40,** 78–82.

Got, J.-L., Frechet, J. & Klein, F.W., 1994. Deep fault plane geometry inferred from multiplet relative relocation beneath the south flank of Kilauea, *J. geophys. Res.,* **99,** 15 375–15 386.

Hao, K.X., Si, H., Fujiwara, H. & Ozawa, T., 2009. Coseismic surface-rupture and crustal deformations of the 2008 Wenchuan earthquake $M_w$ 7.9, China, *Geophys. Res. Lett.,* **36,** L11303 doi:10.1029/2009GL037971.

Ji, C., Shao, G., Lu, Z., Hudnut, K., Jiu, J., Hayes, G. & Zeng, Y., 2008. Rupture history of 2008 May 12 $M_w$ 8.0 Wenchuan earthquake: evidence of slip interaction, *EOS, Trans. Am. geophys. Un.,* **89,** Fall meeting supplement, abs. S23E-02.

Klein, F.W., 2002. User's guide to HYPOINVERSE–2000, a fortran program to solve for earthquake locations and magnitudes. USGS Open-File Report 2002-171, pp. 123, http://pubs.usgs.gov/of/2002/0171/.

Li, L., Chen, Q.-F., Niu, F. & Su, J., 2011. Deep slip rates along the Longmen Shan fault zone estimated from repeating microearthquakes, *J. geophys. Res.,* **116,** B09310, doi:10.1029/2011JB008406.

Liu, Z., Huang, J., Peng, Z. & Su, J., 2014. Seismic velocity changes in the epicentral region of the 2008 Wenchuan earthquake measured from three-component ambient noise correlation techniques, *Geophys. Res. Lett.,* **41,** doi:10.1002/2013GL058682.

Long, H. & Wen, L., 2012. Using repeated sources to quantitatively determine temporal change of medium properties: Theory and an example, *J. geophys. Res.,* **117,** B09303, doi:10.1029/2012JB009302.

Nadeau, R.M., Foxall, W. & McEvilly, T.V., 1995. Clustering and periodic recurrence of microearthquakes on the San Andreas fault at Parkfield, California, *Science,* **267,** 503–507.

Niu, F., Silver, P.G., Nadeau, R.M. & McEvilly, T.V., 2003. Migration of seismic scatterers associated with the 1993 Parkfield aseismic transient event, *Nature,* **426,** 544–548.

Niu, F., Silver, P.G., Daley, T.M., Cheng, X. & Majer, E.L., 2008. Preseismic velocity changes observed from active source monitoring at the Parkfield SAFOD drill site, *Nature,* **454,** 204–208.

Obermann, A., Froment, B., Campillo, M., Larose, E., Planès, T., Valette, B., Chen, J.H. & Liu, Q.Y., 2014. Seismic noise correlations to image structural and mechanical changes associated with the $M_w$ 7.9 2008 Wenchuan earthquake, *J. geophys. Res.,* **119,** 3155–3168.

Peng, Z. & Ben-Zion, Y., 2006. Temporal changes of shallow seismic velocity around the Karadere-Düzce branch of the north Anatolian fault and strong ground motion, *Pure appl. Geophys.,* **163,** 567–600.

Peng, Z. & Zhao, P., 2009. Migration of early aftershocks following the 2004 Parkfield earthquake, *Nat. Geosci.,* **2,** 877–881

Poupinet, G., Ellsworth, W.L. & Frechet, J., 1984. Monitoring velocity variations in the crust using earthquake doublets: an application to the Calaveras Fault, California, *J. geophys. Res.,* **89,** 5719–5731.

Press, W.H., Teukolsky, S.A., Vetterling, W.T. & Flannery, B.P., 1992. *Numerical Recipes in C: The Art of Scientific Computing,* 2nd edn, pp. 661–66, Cambridge Univ. Press.

Rubinstein, J.L. & Beroza, G.C., 2004a. Evidence for widespread nonlinear strong ground motion in the $M_w$ 6.9 Loma Prieta earthquake, *Bull. seism. Soc. Am.,* **94,** 1595–1608.

Rubinstein, J.L. & Beroza, G.C., 2004b. Nonlinear strong ground motion in the ML 5.4 Chittenden earthquake: evidence that preexisting damage increases susceptibility to further damage, *Geophys. Res. Lett.,* **31,** L23614, doi:10.1029/2004GL021357.

Rubinstein, J.L. & Beroza, G.C., 2005. Depth constraints on nonlinear strong ground motion from the 2004 Parkfield earthquake, *Geophys. Res. Lett.,* **32,** L14313, doi:10.1029/2005GL023189.

Rubinstein, J.L., Uchida, N. & Beroza, G.C., 2007. Seismic velocity reductions caused by the 2003 Tokachi-Oki earthquake, *J. geophys. Res.,* **112,** B05315, doi:10.1029/2006JB004440.

Schaff, D.P., 2010. Improvements to detection capability by cross-correlating for similar events: a case study of the 1999 Xiuyan, China, sequence and synthetic sensitivity tests, *Geophys. J. Int.,* **180,** 829–845.

Schaff, D.P. & Beroza, G.C., 2004. Coseismic and postseismic velocity changes measured by repeating earthquakes, *J. geophys. Res.,* **109,** B10302, doi:10.1029/2004JB003011.

Schaff, D.P. & Kim, W.-Y., 2012. A rare foreshock sequence of the 20 January 2007 Odaesan, Korea, earthquake to measure the existence of preseismic velocity changes, *J. geophys. Res.,* **117,** B06314, doi:10.1029/2012JB009232.

Shen, Z.K. *et al.*, 2009. Slip maxima at fault junctions and rupturing of barriers during the 2008 Wenchuan earthquake, *Nat. Geosci*., **2**(10), 718–724.

Silver, P.G., Daley, T.M., Niu, F. & Majer, E.L., 2007. Active source monitoring of crosswell seismic travel time for stress-induced changes, *Bull. seism. Soc. Am.,* **97,** 281–293.

Snieder, R., 2006. The theory of coda wave interferometry, *Pure appl. Geophys.,* **163,** 455–473.

Taira, T., Silver, P.G., Niu, F. & Nadeau, R.M., 2008. Detecting seismogenic stress evolution and constraining fault-zone rheology in the San Andreas Fault following the 2004 Parkfield Earthquake, *J. geophys. Res.,* **113,** B03303, doi:10.1029/2007JB00615.

Waldhauser, F. & Ellsworth, W.L., 2000. A double-difference earthquake location algorithm: Method and application to the Northern Hayward Fault, California. *Bull. seism. Soc. Am.,* **90**(6), 1353–1368.

Wessel, P. & Smith, W.H.F., 1998. New, improved version of the Generic Mapping Tools released, *EOS, Trans. Am. geophys. Un.,* **79**(47), 579.

Xu, X.-W., Wen, X., Yu, G., Chen, G., Klinger, Y., Hubbard, J. & Shaw, J., 2009. Coseismic reverse- and oblique-slip surface faulting generated by the 2008 $M_w$ 7.9 Wenchuan earthquake, China, *Geology,* **37**(6), 515–518.

Yu, W., Song, T.A. & Silver, P.G., 2013. Temporal velocity changes in the crust associated with the great Sumatra earthquakes, *Bull. seism. Soc. Am.,* **103**(5), 2797–2809.

Zhang, Y., Xu, L.S. & Chen, Y.T., 2009. Spatio-temporal variation of the source mechanism of the 2008 great Wenchuan earthquake, *Chin. J. Geophys. (in Chinese),* **52**(2), 379–389.

Zhao, P. & Peng, Z.G., 2009. Depth extent of damage zones around the central Calaveras fault from waveform analysis of repeating earthquakes, *Geophys. J. Int.,* **179,** 1817–1830.

Zhao, C.P., Chen, Z.L., Zhou, L. Q., Li, Z.X. & Kang, Y., 2010. Rupture process of the Wenchuan M8.0 earthquake of Sichuan, China: the segmentation feature, *Chin. Sci. Bull.,* **55**(3), 284–292.